Density functional theory investigation of 3*d*, 4*d*, and 5*d* 13-atom metal clusters

Maurício J. Piotrowski and Paulo Piquini
Departamento de Física, Universidade Federal de Santa Maria, Santa Maria 97105-900, RS, Brazil

Juarez L. F. Da Silva*
Instituto de Física de São Carlos, Universidade de São Paulo, Cx. Postal 369, São Carlos 13560-970, SP, Brazil
(Received 2 October 2009; revised manuscript received 5 February 2010; published 22 April 2010)

The knowledge of the atomic structure of clusters composed by few atoms is a basic prerequisite to obtain insights into the mechanisms that determine their chemical and physical properties as a function of diameter, shape, surface termination, as well as to understand the mechanism of bulk formation. Due to the wide use of metal systems in our modern life, the accurate determination of the properties of 3*d*, 4*d*, and 5*d* metal clusters poses a huge problem for nanoscience. In this work, we report a density functional theory study of the atomic structure, binding energies, effective coordination numbers, average bond lengths, and magnetic properties of the 3*d*, 4*d*, and 5*d* metal (30 elements) clusters containing 13 atoms, M_{13}. First, a set of lowest-energy local minimum structures (as supported by vibrational analysis) were obtained by combining high-temperature first-principles molecular-dynamics simulation, structure crossover, and the selection of five well-known M_{13} structures. Several new lower energy configurations were identified, e.g., Pd_{13}, W_{13}, Pt_{13}, etc., and previous known structures were confirmed by our calculations. Furthermore, the following trends were identified: (i) compact icosahedral-like forms at the beginning of each metal series, more opened structures such as hexagonal bilayerlike and double simple-cubic layers at the middle of each metal series, and structures with an increasing effective coordination number occur for large *d* states occupation. (ii) For Au_{13}, we found that spin-orbit coupling favors the three-dimensional (3D) structures, i.e., a 3D structure is about 0.10 eV lower in energy than the lowest energy known two-dimensional configuration. (iii) The magnetic exchange interactions play an important role for particular systems such as Fe, Cr, and Mn. (iv) The analysis of the binding energy and average bond lengths show a paraboliclike shape as a function of the occupation of the *d* states and hence, most of the properties can be explained by the chemistry picture of occupation of the bonding and antibonding states.

DOI: 10.1103/PhysRevB.81.155446 PACS number(s): 61.46.Bc, 61.46.Df, 61.50.Ah, 61.82.Bg

I. INTRODUCTION

Particles/clusters containing few to thousand atoms show chemical and physical properties[1–3] that are different from those observed for their bulk counterparts.[4] In particular, several studies have found that the structural, optical, magnetic, and reactivity of clusters are greatly dependent on their diameter, shape, and surface termination. Thus, clusters with specific properties can be designed by tuning particle size, shape, and surface termination in high controlled experiments,[5] which opens the possibility for a wide range of technological applications in nanoscience. Furthermore, clusters containing few atoms are considered the basic building blocks of macroscopic systems and hence, the study of clusters can provide insights into the formation mechanism of macroscopic systems.

For example, gold particles with macroscopic size are not active for catalysis applications. However, gold particles with about 1.5 nm (about 55 atoms) show unexpected catalytic behavior for several reactions.[6] Furthermore, gold nanoparticles have been studied for selective release of multiple drugs in combination therapy.[7] These findings have motivated a large number of studies to understand the origin of the catalytic activity of gold clusters containing few atoms (7–55).[8–11] However, a simple explanation of the catalytic properties of gold nanoparticles is still far from satisfactory, which can be attributed to the difficulties to obtain a complete knowledge of the atomic structure of gold clusters in gas phase[11] or ligand-protected clusters.[11,12]

It is well known that macroscopic particles of Pt, Pd, and Rh supported on oxides compounds, e.g., $CeO_{2-x}(0<x<1/2)$,[13–16] are widely used as active components in catalysis, e.g., three-way catalysts,[17] ethanol electro-oxidation.[18,19] The transition-metal components represent a substantial part of the manufacturer cost of a catalytic devices, and the use of nanoparticles provide the possibility to wisely select the particles size and shape that are the most cost efficient for catalytic applications.[20] Thus, there are great expectations that nanoparticles can contribute to increase efficiency and reduce the cost of catalytic devices.

Recently, experimental studies have identified that nanoparticles of Rh confined in carbon nanotubes enhance ethanol production compared with oxide supported large Rh particles.[21] Experimental studies have found that even Pt clusters with subnanometer size (8–9 atoms), stabilized on high-surface-area substrates (Al_2O_3), are 40–100 times more active for the oxidative dehydrogenation of propane than previously studied Pt and vanadia catalysts.[22] It is important also to mention that Pt, Pd, Rh, and Au have been used in core-shell nanoparticles to design new catalysts, which combine the properties of two or more systems.[23–28]

Experimental and theoretical studies have suggested that Al_{13} acts like a superhalogen atom.[29] It shows that highly stable clusters can exhibit unique properties. Also, Al clusters with few atoms (16–18) have been suggested as catalysts

for H_2 generation by water splitting.[30] Transition-metal elements that are *nonmagnetic* on their bulk phase can show unexpected large magnetic moments for particles with few atoms, e.g., $Rh_n(n=12-32)$ (Refs. 31–35) while *magnetic* bulk materials exhibit an enhancement of their magnetic moments at nanoscale.[36,37] This have great importance in the field of magnetic storage and spintronics.

Experimental studies employing time-of-flight mass spectrometry for clusters[1–3] have shown that clusters with a particular number of atoms (magic number) occur more often, which indicates higher relative stability for those clusters. For example, clusters with 13 atoms have a high rate of occurrence for Fe, Ti, Zr, Nb, Ta, and Al,[30,38] which have been supported by first-principles calculations.[39,40] Furthermore, structural model analysis based on close-packed icosahedral (ICO) configurations would favor clusters with 13, 55, and 147 atoms,[41] however, this analysis does not take into account the nature of the chemical bonds among the different systems and hence, different magic numbers are also possible. Thus, the identification of magic number clusters might play an important role to understand their stability as a function of particle size.

The main problem to obtain a deep atomic-level understanding of the physical and chemical properties of clusters relies on an accurate determination of their equilibrium atomic structure, which is not simple to be obtained as might appear. A direct identification of the equilibrium atomic structure by experimental techniques is very difficult and only indirect measurements can provide few clues about the underlying atomic structure. Thus, the combination of experimental techniques with first-principles calculations has been used. For example, vibrational spectroscopy combined with theoretical calculations has lead to important insights into the atomic structure of Au clusters.[10]

Magnetic properties of isolated metal clusters have been investigated by Stern-Gerlach molecular-beam deflection experiments[31,34,36,42–45] and a large number of data, e.g., total magnetic moments, have been reported. These data have been useful as a guide line in the identification of the atomic structure by first-principles calculations. For example, the atomic structure of Rh_{13} have been revealed only after a search for atomic configurations[46] with lower total magnetic moments reported in experimental studies.[31,33] However, the combination of magnetic experiments with first-principles calculations to identify equilibrium structures have its own problems. It can be applied only for systems with a strong dependence of the magnetic moment on the atomic configurations, which is not the case for most of the systems. For example, Pt, Cu, Au, etc., have an almost constant magnetic moment for different atomic configurations.

As mentioned above, experimental techniques have found difficulties to identify directly the atomic structure of clusters. Thus, most of the structural studies have been based on theoretical calculations, which can determine directly the atomic structure of clusters using several well-defined algorithms. Magic number clusters have high relative stability and hence, it has great importance. Several recent first-principles calculations based on density functional theory (DFT) have focused on those clusters, in particular, on metal particles containing 13 atoms. For example, Sc_{13},[39,47] Ti_{13},[48] V_{13},[49,50] Cr_{13},[51] Mn_{13},[52,53] Fe_{13},[54–57] Co_{13},[40,57–65] Ni_{13},[57,64,66–70] Cu_{13},[62,65,70–75] Zn_{13},[76–78] Y_{13},[62,78,79] Zr_{13},[62,78,79] Nb_{13},[62,78–80] Mo_{13},[62,78,79] Tc_{13},[62,65,78,79] Ru_{13},[32,62,65,78,81] Rh_{13},[32,46,62,64,65,78,82–87] Pd_{13},[32,62,64,65,70,78,87–91] Ag_{13},[62,65,70,72,73,78,87,92] Cd_{13},[62,76,78,93] Lu_{13},[94] Ta_{13},[78] W_{13},[78] Re_{13},[65,78] Os_{13},[65,78] Ir_{13},[62,65,78,95] Pt_{13},[62,65,69,70,78,88,96–98] Au_{20},[62,65,70,72,73,99–103] and Hg_{13}.[104,105] It can be noticed that particular systems have been widely studied, e.g., Rh_{13}, Pd_{13}, Ag_{13}, Pt_{13}, and Au_{13} while other systems have rarely been studied, e.g., Cr_{13}.

Almost all previous works, with few exceptions,[78] focused on just one or few particular systems, i.e., there is no study that include all the $3d$, $4d$, and $5d$ M_{13} clusters. Furthermore, it is important to mention that few works have focused in the search for lowest-energy structures while most of the studies have assumed predefined structures. Therefore, although several studies have been performed, a basic understanding of the structure and electronic properties as a function of the atomic number for the $3d$, $4d$, and $5d$ systems remains incomplete and further studies are highly desirable due to the wide importance of clusters in nanoscience.

In order to understand the structure and electronic trends as a function of the occupation of the d states (atomic number), as well as to provide a comprehensive comparative analysis of all the $3d$, $4d$, and $5d$ systems, we studied the atomic and electronic structure properties of all $3d$, $4d$, and $5d$ M_{13} clusters (30 systems) employing first-principles calculations. We identified a set of lowest-energy atomic configurations, whose local minimum character has been confirmed by vibrational analysis. For particular systems such as Ni_{13}, Pd_{13}, W_{13}, Pt_{13}, etc., we identified new lower energy configurations compared with previous studies. Thus, this work provides one of the most complete set of lowest-energy configurations for the $3d$, $4d$, and $5d$ M_{13} clusters.

In order to obtain quantitative insights into the atomic structure trends, we calculated the binding energy, effective coordination number (ECN), average bond lengths, total magnetic moment, and vibrational frequencies. From those results, we identified the trends along of the $3d$, $4d$, and $5d$ series. (i) Compact icosahedral-like forms at the beginning of each metal series and more opened structures, such as hexagonal bilayer (HBL)-like and double simple cubic (DSC) layer, forms at the middle of each metal series and an effective coordination increasing is observed for large d states occupation. (ii) For Au_{13}, we found that spin-orbit coupling (SOC) favors the three-dimensional (3D) structures, i.e., our 3D structure is about 0.10 eV lower in energy than the lowest energy known two-dimensional (2D) configuration. (iii) The magnetic exchange interactions play an important role for particular systems such as Fe, Cr, and Mn. (iv) The analysis of the binding energy and average bond lengths show a paraboliclike shape as a function of the occupation of the d states and hence, most of the properties can be explained by the chemistry picture of occupation of the bonding and antibonding states. The remaining of this paper is organized as follows: In Sec. II, we show the theoretical approach and computational details. The results are reported in Sec. III. Section IV contains a discussion and our conclusions.

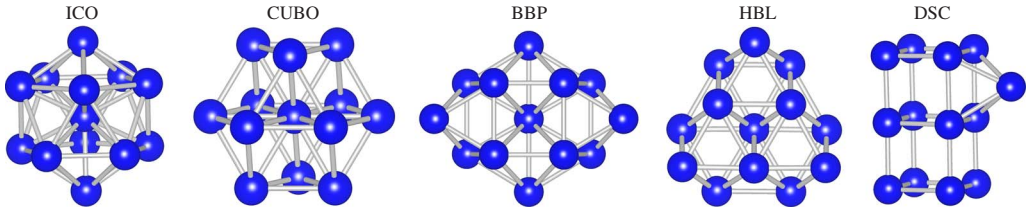

FIG. 1. (Color online) Symmetric configurations calculated for the M_{13} clusters, namely, ICO, CUBO, BBP, HBL, and DSC.

II. THEORETICAL APPROACH AND COMPUTATIONAL DETAILS

A. Total-energy calculations

Our spin-polarized first-principle calculations for the 3*d*, 4*d*, and 5*d* metal clusters with 13 atoms, M_{13}, are based on DFT (Refs. 106 and 107) within the generalized gradient approximation[108] formulated by Perdew, Burke, and Ernzerhof (PBE) (Ref. 109) to the exchange-correlation energy functional (from now DFT-PBE). The Kohn-Sham equations are solved employing the all-electron projected augmented wave (PAW) method,[110,111] as implemented in the Vienna *ab initio* simulation package (VASP).[112,113] We used the PAW projectors as provided within VASP (Ref. 111) and hence, SOC effects are not directly taken into account for the valence electrons. It has been known that SOC might affect the relative total energy among different isomers of heavy elements clusters, e.g., Pt, Au, and Hg.[100,114] Thus, to understand the effect of the SOC in the atomic structure of M_{13} clusters composed by heavy elements, additional calculations with the SOC for the valence states as implemented in VASP (from now DFT-PBE+SOC) were also performed for all the 4*d* and 5*d* systems.

We considered all PAW projectors for which the semicore electrons are taken into account as valence electrons. For the cutoff energies, we employed the recommended values in the PAW projectors (ENMAX), i.e., cutoff energies from 150 eV to about 380 eV. For all calculations, the equilibrium geometries are obtained when the atomic forces are smaller than 0.010 eV/Å and the total energy converges within 10^{-6} eV. All calculations were performed with a cubic box of 17 Å and using a single **k** point (Γ point) for the Brillouin-zone (BZ) integration. In order to check the accuracy of our results, selected calculations were also performed using a cubic box of 20 Å, as well as a larger number of **k** points, e.g., $(2\times2\times2)$ (8 **k** points in BZ). We found negligible differences in the results and hence, we report only calculations performed using a cubic box of 17 Å and a single **k** point. For the binding-energy calculations, the free atoms were calculated employing an orthorhombic box with dimensions of $17\times17.25\times17.50$ Å^3 with a single **k** point (Γ point) for the BZ integration.

B. Atomic structure generation

It is well known that even a simple M_{13} cluster contains thousands of local minimum configurations and it increases almost exponentially with the number of atoms.[3] Thus, sophisticated algorithms have been employed in the search for the lowest-energy structures, namely, genetic algorithm (GA),[115] basin-hopping Monte Carlo (BHMC),[63,103,116,117] Monte Carlo (MC),[71] conformational space annealing,[87] taboo search in descriptor space (TSDS),[78,118] and high-temperature (high-*T*) molecular dynamics (MD).[65] For almost all studies, GA, BHMC, MC, and TSDS algorithms are combined with empirical pair potentials due to the high computational cost of those algorithms (large number of evaluated configurations).[116,117] However, empirical pair potentials have difficulties to provide a correct description of the atomic structure of nanoclusters[3] and hence, its ground-state structure might not be correct.

The use of first-principles calculations combined with algorithms such as GA and BHMC is prohibitive for a complete study of 30 elements due to the extreme large number of configurations that must be evaluated in order to obtain the ground-state structure.[116] Thus, in this work, we use a set of approaches in order to obtain a reliable set of lowest-energy structures, which will be used to discuss structural and electronic trends along of the 3*d*, 4*d*, and 5*d* series.

First, we employed high-*T* MD simulations as a structure generator to yield structure inputs for conventional total-energy minimizations (conjugated gradient schemes). For those MD calculations, a time step of 2–4 fs was used for all calculations, with MD runs being about 30–60 ps long, along which the following procedure was adopted. A disordered structure was selected and heated during few picosecond above melting temperature in order to remove any symmetry history. Then, the system was cooled down up to a particular temperature and a constant-temperature MD run was performed for few picosecond. This procedure was repeated until zero temperature is reached. Snapshots (atomic configurations) were collected along with the complete simulation, quenched to zero temperature, and optimized.

We found that our high-*T* MD simulations have difficulties to generate high-symmetry configurations, e.g., icosahedron. It can be attributed to the relatively short time scale of our simulations. However, it is well known that several elements in the periodic table have high-symmetry ground-state structures for M_{13}. Thus, we included five widely known M_{13} structures with high symmetry, Fig. 1, in our calculations, namely, ICO (I_h),[3,41] cuboctahedron (CUBO, O_h),[3] buckled biplanar (BBP, C_{2v}),[62] HBL (C_{3v}),[40,65,78,119] and the double simple cubic (DSC).[65,78,95] These high-symmetry configurations were selected by their topology (close-packed, layered, and open structures) and energetics based on DFT calculations.[40,46,62] The geometry optimizations for the high-symmetry clusters were performed with and without symmetry constraints in order to identify possible symmetry breaking.

It has been known that several nearby elements in the periodic table have the same ground-state structure, e.g., Rh,

Pd, and Ag crystallize in the same face-centered-cubic structure.[4] Thus, we expect that a similar trend could also be true for clusters. In this way, structural crossover was performed among different systems. For example, we selected the lowest-energy structure identified for Rh_{13} as a starting configuration for other systems in the periodic table. Different spin configurations were taking into account in our calculations, e.g., ferromagnetic (FM), antiferromagnetic (AFM), and ferrimagnetic (FIM) orderings. This is particularly important for particular systems, e.g., V_{13}, Cr_{13}, Mn_{13}, etc. Finally, MD simulations at 300 K were performed for selected systems to check their stability.

We would like to stress that the five configurations shown in Fig. 1 are the only external structures employed in this work, i.e., all other configurations are obtained using the procedures described above. All relative energy differences, binding energies, and magnetic moments are given per cluster.

III. RESULTS AND DISCUSSION

First, using the procedure outlined above, we calculated about 15–45 configurations for each M_{13} system without taken into account SOC effects for the valence electrons, i.e., DFT-PBE calculations. Second, in order to understand the role played by SOC in the atomic structure of heavy element M_{13} clusters, we selected a set of six structures, namely, the ICO, CUBO, BBP, HBL, DSC, and the lowest-energy configurations and additional geometric optimizations were performed by taken into account SOC effects for the valence states (DFT-PBE+SOC). Thus, a set of lowest-energy configurations were identified and the following properties were calculated, namely, relative total energies, binding energies, effective coordination number, average bond lengths, total magnetic moments, and vibrational frequencies.

A. Relative energy stability

The relative energies of all M_{13} clusters, ΔE_{tot}, with respect to the total energy of the ideal ICO cluster, $E_{\text{tot}}^{\text{ICO}}$, are calculated as

$$\Delta E_{\text{tot}} = E_{\text{tot}}^{\text{cluster}} - E_{\text{tot}}^{\text{ICO}}, \tag{1}$$

where $E_{\text{tot}}^{\text{cluster}}$ is the total energy of a particular configuration. The results for ΔE_{tot} for all systems and configurations are shown in Fig. 2 while the results for the CUBO, BBP, HBL, DSC, and the lowest-energy configurations are summarized in Table I. A negative (positive) value of ΔE_{tot} indicates a cluster with energy lower (higher) than the ideal ICO cluster.

We found that the magnitude of the relative energy difference between the lowest- and highest-energy configurations shows a strong dependence on the occupation of the *d* states, which could be attributed to the selected structures. However, we want to point out that compact (ICO) and open (DSC) structures were calculated for all systems and hence, the magnitude of the relative energy differences can provide some insights. For example, for elements with a large occupation of the *d* states, such as Co, Ni, Cu, Zn, Rh, Pd, Ag, Cd, Au, and Hg, the energy difference between the lowest- and highest-energy clusters is smaller than 2.50 eV. However, most of the remaining systems with small occupation of the *d* states have energy differences of about 4.0–7.0 eV. We found also particular cases, e.g., Hg_{13}, for which the energy difference between the lowest (compact)- and highest (open)-energy configuration is 0.37 eV, which can be explained by the weak van der Waals interaction between the Hg atoms.[104]

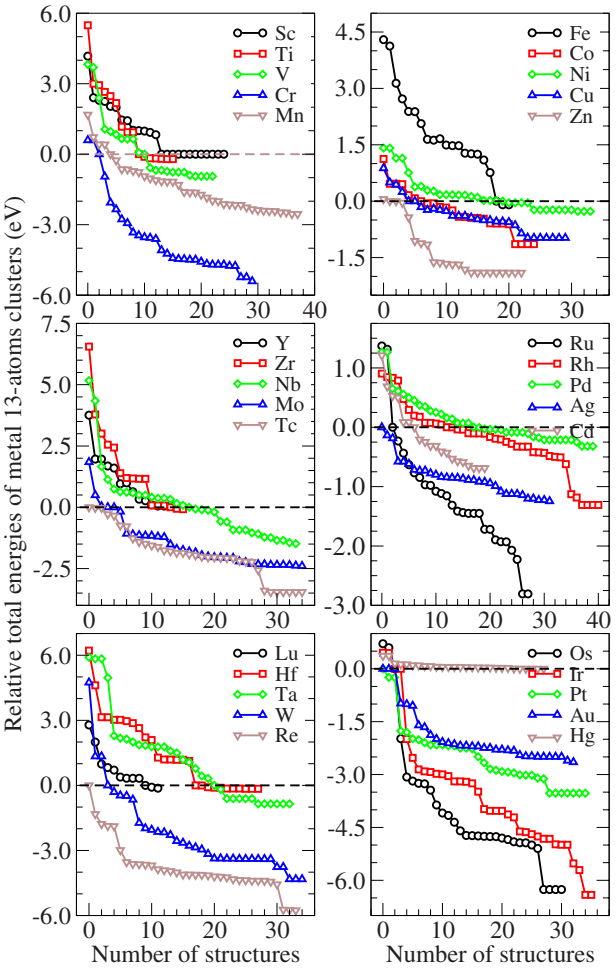

FIG. 2. (Color online) Relative total energies, ΔE_{tot}, for all calculated M_{13} configurations with respect to the ideal ICO M_{13} cluster (dashed horizontal lines). $\Delta E_{\text{tot}} = E_{\text{tot}}^{\text{cluster}} - E_{\text{tot}}^{\text{ICO}}$.

B. Binding energy

In order to obtain further insights, we calculated the binding energy per atom for the lowest-energy clusters, E_{b}, which is given by

$$E_{\text{b}} = E_{\text{tot}}^{\text{lowest}} - E_{\text{tot}}^{\text{free-atom}}, \tag{2}$$

where $E_{\text{tot}}^{\text{lowest}}$ is the total energy per atom of the lowest-energy configuration while $E_{\text{tot}}^{\text{free-atom}}$ is the total energy of the free atom. The results are shown in Fig. 3. We found that the binding energy as a function of the atomic number shows a similar shape as compared to the cohesive energy of the respective solids, as it is discussed in material science books (see Ref. 120). Even the peaks observed for Cr, Mn, and Mo

TABLE I. Relative total energies (in electron volt) and total magnetic moments (in μ_B) calculated without SOC for the valence states.

ΔE_{tot}	Sc	Ti	V	Cr	Mn	Fe	Co	Ni	Cu	Zn
ICO	0.00 (19)	0.00 (6)	0.00 (7)	0.00 (20)	0.00 (33)	0.00 (44)	0.00 (31)	0.00 (8)	0.00 (5)	0.00 (0)
CUBO	+2.40 (3)	+2.65 (10)	+3.70 (15)	+0.60 (4)	+0.41 (47)	+2.39 (40)	+0.46 (27)	+1.15 (6)	+0.50 (1)	+0.06 (0)
DSC	+4.17 (5)	+5.49 (2)	+3.82 (1)	−0.95 (12)	+1.68 (43)	+4.30 (40)	+1.12 (27)	+1.41 (10)	+0.88 (1)	−0.43 (2)
BBP	+2.04 (7)	+2.47 (2)	+2.39 (11)	−2.06 (20)	+0.72 (41)	+1.48 (40)	−0.47 (25)	+0.13 (10)	−0.44 (1)	−1.06 (0)
HBL	+2.25 (5)	+2.94 (2)	+0.97 (9)	−3.45 (14)	−1.17 (29)	+1.65 (40)	−1.14 (27)	+0.16 (12)	−0.39 (1)	−1.11 (0)
Lowest	0.00 (19)	−0.21 (6)	−0.94 (1)	−5.41 (0)	−2.55 (3)	−0.10 (44)	−1.14 (27)	−0.27 (10)	−0.98 (1)	−1.90 (0)

ΔE_{tot}	Y	Zr	Nb	Mo	Tc	Ru	Rh	Pd	Ag	Cd
ICO	0.00 (19)	0.00 (6)	0.00 (3)	0.00 (10)	0.00 (13)	0.00 (12)	0.00 (17)	0.00 (8)	0.00 (5)	0.00 (0)
CUBO	+1.97 (3)	+3.79 (10)	+4.34 (1)	+0.04 (2)	−0.74 (5)	+1.37 (18)	+0.85 (19)	+0.65 (6)	−0.14 (1)	+0.09 (0)
DSC	+3.76 (3)	+6.55 (0)	+5.17 (1)	+1.85 (0)	−1.27 (3)	−2.81 (4)	−1.31 (9)	+1.27 (6)	−1.08 (1)	+0.53 (0)
BBP	+1.60 (7)	+2.55 (2)	+0.74 (1)	−1.08 (2)	−1.61 (5)	−0.85 (6)	−0.20 (17)	−0.01 (4)	−0.80 (1)	−0.31 (0)
HBL	+1.68 (5)	+3.01 (2)	+0.37 (3)	−1.16 (2)	−3.46 (1)	−1.72 (8)	−0.25 (5)	−0.18 (2)	−0.73 (1)	−0.21 (0)
Lowest	0.00 (19)	−0.08 (6)	−1.48 (1)	−2.57 (0)	−3.46 (1)	−3.20 (2)	−1.31 (9)	−0.32 (6)	−1.25 (1)	−0.69 (0)

ΔE_{tot}	Lu	Hf	Ta	W	Re	Os	Ir	Pt	Au	Hg
ICO	0.00 (13)	0.00 (6)	0.00 (7)	0.00 (6)	0.00 (13)	0.00 (2)	0.00 (11)	0.00 (2)	0.00 (5)	0.00 (0)
CUBO	+2.00 (5)	+3.14 (4)	+4.96 (3)	−0.47 (2)	−1.87 (7)	+0.71 (2)	+0.46 (19)	−0.24 (6)	−0.98 (1)	+0.05 (0)
DSC	+2.78 (3)	+6.21 (0)	+5.84 (3)	+1.34 (0)	−3.54 (1)	−6.26 (4)	−6.41 (3)	−2.25 (4)	−1.00 (1)	+0.37 (0)
BBP	+0.82 (7)	+2.21 (2)	+1.18 (1)	−1.98 (2)	−3.69 (7)	−3.44 (4)	−2.98 (3)	−2.01 (4)	−1.88 (1)	+0.08 (0)
HBL	+0.98 (5)	+3.02 (2)	+2.18 (1)	−2.05 (0)	−5.76 (5)	−4.75(4)	−3.19(11)	−2.16 (0)	−2.24 (1)	+0.06 (0)
Lowest	−0.13 (13)	−0.16 (6)	−0.85 (1)	−4.32 (0)	−5.76 (5)	−6.26(4)	−6.68(3)	−3.53 (2)	−2.65 (1)	0.00 (0)

are well reproduced by our lowest-energy clusters. Thus, the same mechanisms used to explain these trends in bulk phase might be applied for M_{13} clusters, however, size effects combined with d states occupation might play a role as well. For example, with few exceptions, all the 3d, 4d, and 5d bulk systems have compact bulk structures, however, several M_{13} clusters, e.g., Ir, Ru, and Rh, have open structures (see below).

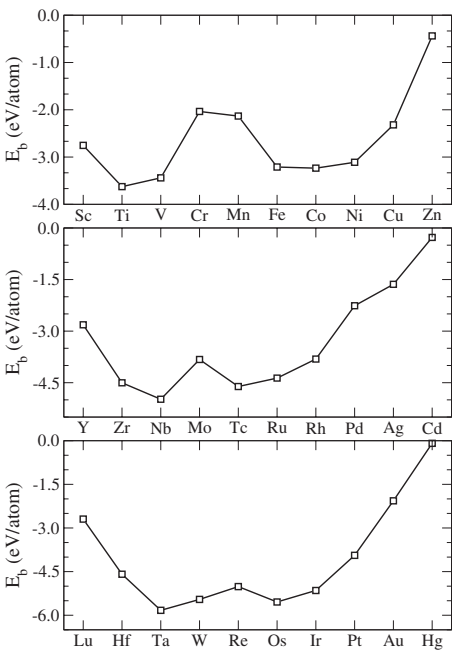

FIG. 3. Binding energy of the M_{13} clusters in their lowest-energy configurations, E_b.

C. Spin-orbit coupling effects in the atomic structure

In order to check the effect of SOC for the heavy M_{13} clusters, we performed additional calculations (DFT-PBE+SOC) for six selected structures (ICO, CUBO, DSC, BBP, HBL, and lowest energy) for the 4d and 5d systems. Those structures were initially optimized without SOC (DFT-PBE), Table I. Thus, DFT-PBE+SOC calculations were performed for fixed DFT-PBE geometries and then, we optimized those structures with DFT-PBE+SOC. The results are summarized in Table II. We found that unrelaxed and fully relaxed clusters with DFT-PBE+SOC yield about the same relative energy differences with respect the unrelaxed ideal ICO configuration, i.e., atomic relaxations within SOC for the valence states can be neglected at least for the majority of the 4d and 5d M_{13} clusters. This observation can be useful due to the high cost of geometry optimization with DFT-PBE+SOC.

For the 4d systems the relative energy differences are about the same with DFT-PBE and DFT-PBE+SOC, however, ΔE_{tot} slightly changes for few 5d systems, which could be expected. For Pt_{13} and Au_{13}, ΔE_{tot} changes by about 0.42

TABLE II. Relative total energies (in electron volt) and total magnetic moments (in μ_B) calculated with SOC for the valence states. The numbers in parentheses are SOC calculations (DFT-PBE+SOC) for fixed atomic configurations obtained without SOC.

ΔE_{tot}	Y	Zr	Nb	Mo	Tc	Ru	Rh	Pd	Ag	Cd
ICO	0.00	0.00	0.00	0.00	0.00	0.00	0.00	0.00	0.00	0.00
CUBO	(+1.97)	(+3.82)	(+4.38)	(+0.03)	(−0.78)	(+1.39)	(+0.78)	(+0.65)	(−0.13)	(+0.08)
	+1.97	+3.82	+4.32	−0.02	−0.79	+1.34	+0.78	+0.56	−0.13	+0.08
DSC	(+3.79)	(+6.55)	(+5.21)	(+1.85)	(−1.28)	(−2.77)	(−1.34)	(+1.32)	(−1.07)	(+0.49)
	+3.76	+6.54	+5.21	+1.84	−1.28	−2.77	−1.34	+1.32	−1.07	+0.49
BBP	(+1.60)	(+2.59)	(+0.78)	(−1.06)	(−1.61)	(−0.82)	(−0.27)	(+0.01)	(−0.79)	(−0.32)
	+1.60	+2.59	+0.69	−1.06	−1.61	−0.82	−0.27	+0.01	−0.79	−0.32
HBL	(+1.69)	(+3.04)	(+0.41)	(−1.15)	(−3.46)	(−1.67)	(−0.52)	(−0.16)	(−0.72)	(−0.21)
	+1.69	+3.04	+0.41	−1.15	−3.46	−1.73	−0.58	−0.20	−0.72	−0.21
Lowest	(0.00)	(−0.05)	(−1.44)	(−2.56)	(−3.47)	(−3.14)	(−1.34)	(−0.29)	(−1.23)	(−0.69)
	0.00	−0.05	−1.44	−2.56	−3.47	−3.16	−1.34	−0.29	−1.23	−0.69

ΔE_{tot}	Lu	Hf	Ta	W	Re	Os	Ir	Pt	Au	Hg
ICO	0.00	0.00	0.00	0.00	0.00	0.00	0.00	0.00	0.00	0.00
CUBO	(+2.00)	(+3.20)	(+4.87)	(−0.33)	(−1.99)	(+0.40)	(+0.33)	(−0.16)	(−0.93)	(+0.05)
	+1.97	+3.20	+4.87	−0.38	−2.00	+0.39	+0.32	−0.21	−0.95	+0.05
DSC	(+2.72)	(+6.26)	(+5.92)	(+1.53)	(−3.58)	(−6.19)	(−6.38)	(−1.78)	(−0.85)	(+0.37)
	+2.64	+6.26	+5.92	+1.53	−3.58	−6.20	−6.38	−1.78	−0.85	+0.37
BBP	(+0.84)	(+2.27)	(+1.25)	(−1.81)	(−3.68)	(−3.42)	(−3.25)	(−1.83)	(−1.71)	(+0.07)
	+0.84	+2.27	+1.25	−1.81	−3.68	−3.44	−3.26	−1.85	−1.71	+0.07
HBL	(+0.99)	(+3.07)	(+2.25)	(−1.86)	(−5.82)	(−4.72)	(−3.26)	(−1.75)	(−2.04)	(+0.05)
	+0.99	+3.07	+1.79	−1.93	−5.84	−4.73	−3.27	−1.78	−2.04	+0.05
Lowest	(−0.11)	(−0.12)	(−0.77)	(−4.12)	(−5.82)	(−6.19)	(−6.57)	(−3.10)	(−2.31)	(0.00)
	−0.11	−0.12	−0.77	−4.12	−5.84	−6.20	−6.58	−3.11	−2.34	0.00

and 0.31 eV, respectively, while it is smaller than 0.20 −0.10 eV for almost all the remaining 5*d* systems. Thus, the most affected systems are Pt and Au, which could be expected due to their large atomic number and incomplete *d* shell. However, it is important to mention that Hg has an even large atomic number but the relative energy differences are not affected by SOC.

For atomic configurations in which the relative energy difference are about 0.10 eV, we noticed a change in the relative stability among the structures for few systems, however, it is important to notice that the relative energy difference between compact and open M_{13} structures are in the range from 2.5 to 7.0 eV (except for Hg_{13}). Thus, it is unlikely that SOC can change the relative stability at this particular energy range, which is supported by our results summarized in Table II. Thus, we should focus our attention only to the cases in which we have very different atomic configurations with a relative energy difference of about 0.10 eV.

We found only a particular case in which SOC plays an important role for the atomic structure of M_{13}, namely, 2D versus 3D structures of Au_{13}. It has been reported that anionic Au clusters with few atoms have a strong preference for planar structures,[102] which is in accordance with our results without SOC for neutral Au_{13}. For example, we found that our lowest 2D configuration is 0.15 eV lower in energy than the lowest 3D configuration. However, the relative stability of the 2D and 3D structures change when SOC is taken into account for the valence states, i.e., the 3D configuration turns 0.10 eV lower in energy than the 2D planar structure, which is consistent with experimental observations.[102] Thus, SOC plays an important role in the stabilization of the 3D configuration for Au_{13} and would be interesting to understand the role of SOC in the competition between 2D and 3D clusters for smaller Au particles. Among all studied cluster with 13 atoms, Au_{13} is the only system in which there is a clear competition of 2D versus 3D structures.

D. Atomic structure

From the results shown in Fig. 2, and Tables I and II, we identified the lowest-energy structures for all M_{13} systems, which are shown in Fig. 4. We found that only three systems have ideal ICO configuration, namely, Sc_{13}, Y_{13}, and Hg_{13} while distorted ICO clusters are found for eight systems, namely, Ti_{13}, V_{13}, Cr_{13}, Mn_{13}, Fe_{13}, Zr_{13}, Lu_{13}, and Hf_{13}. Therefore, we can conclude that the 3*d* systems have a larger preference for close-packed structures than the 4*d* and 5*d* systems. The energy gain due to the distortions is less than 0.25 eV for Ti_{13}, Fe_{13}, Zr_{13}, Lu_{13}, and Hf_{13} while the same is not the case for V_{13}, Cr_{13}, and Mn_{13}, e.g., an energy gain of 0.9, 5.4, and 2.6 eV for V_{13}, Cr_{13}, and Mn_{13}, respectively, which can be mainly attributed to the FIM magnetic interac-

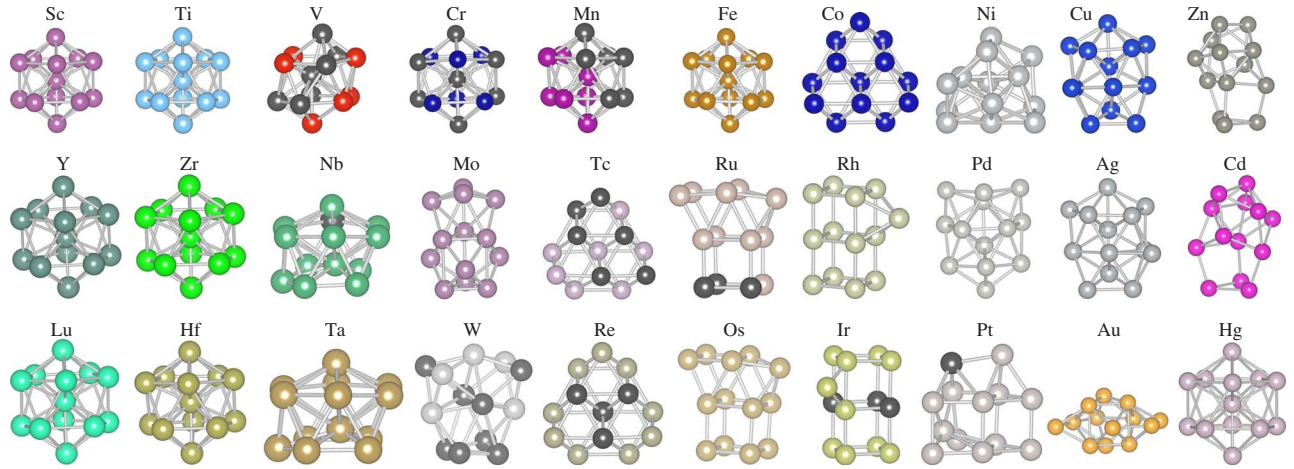

FIG. 4. (Color online) Lowest-energy structures for the M_{13} systems. Configurations in which there are two atom colors, it indicates positive and negative (black atoms) local magnetic moments located in the respective atom.

tions and atomic distortions. It is important to notice that Mn_{13} has very likely an ICO-like structure while V_{13} and Cr_{13} show apparently large distortions.

For Nb_{13} and Ta_{13}, we noticed that two extra atoms can be added to the structure to form a compact structure with 15 atoms, which might have greater stability than the M_{13} cluster. Both V, Nb, and Ta elements are located in the same column (group V) and hence, we would expect that V_{13} or even other elements nearby the group V could have similar structure. We found that the lowest-energy structures for V_{13} and Cr_{13} have empty space to add one (V_{13}) or two (Cr_{13}) extra atoms to form a similar compact 15-atom structure. Thus, it might explain the large distortions observed in V_{13} and Cr_{13} compared with the ideal ICO structure, i.e., both V_{13} and Cr_{13} have structures between the distorted ICO and a compact 15-atom structure. It is important to mention that the Nb_{13} and Ta_{13} configurations were obtained by high-T MD simulations starting from a distorted ICO cluster, i.e., no previous information was used even though previous results have reported this structure for Ta_{13}.[78]

Among the 3d, 4d, and 5d systems, we found that only Co_{13}, Tc_{13}, and Re_{13} have an ideal HBL structure (C_{3v}). The ideal HBL structure is composed by two coplanar hexagonal layers with a close-packed stacking, which can be related with their bulk hexagonal close-packed structures.[4] The ideal HBL and CUBO clusters differ only by the position of three atoms, which are located below the seven-atom hexagonal layer in the CUBO cluster. Furthermore, HBL differs from the BBP in the atomic positions in the second layer, which forms a square of four atoms capped by two atoms at the opposite edges in the BBP cluster. We would like to point out that a structure very similar to the HBL was obtained independently by our high-T MD simulations for Tc_{13}, which is only slightly higher in energy (about 0.30 eV).

The HBL structure was also reported for Re_{13},[78] which is consistent with our results. Furthermore, it was recently obtained by DFT calculations that HBL is about 0.72 eV lower in energy than BBP for Co_{13} (Ref. 40) while we obtained 0.67 eV, Table I. The HBL and BBP structures are almost degenerate (energy difference less than 0.05 eV) for several systems, e.g., Ni_{13}, Cu_{13}, Zn_{13}, Y_{13}, Mo_{13}, Rh_{13}, Ag_{13}, Cd_{13}, W_{13}, and Hg_{13}, which can be expected due to the small geometric differences. It is important to mention that this result depends on a full relaxation on both HBL and BBP structures without symmetry constrain.

In contrast with previous DFT calculations,[62] we found that the BBP configuration is not the lowest configuration for any of the 3d, 4d, and 5d M_{13} systems, i.e., it is only a high-energy local minimum structure. In previous studies,[62] the stability of the BBP structure was verified by room-temperature MD simulations, which might not be sufficient to provide enough energy for structural change along of the simulation. Thus, MD simulations should be used with caution to check structure stability, as the appropriate temperature depends on the shape of the potential-energy surface.

We found that the Cu_{13}, Pd_{13}, and Ag_{13} systems have a distorted HBL structure, which is composed by two layers as in the ideal HBL structure, but only three atoms preserve their atomic positions in the second layer. The distorted HBL Cu_{13}, Pd_{13}, and Ag_{13} structures are 0.59, 0.14, and 0.52 eV lower compared to HBL, respectively. Thus, it can be suggested that Cu_{13} and Ag_{13} have ordered structures, which is in contrast with previous DFT calculations that reported only disordered structures for Cu_{13} and Ag_{13}.[72] In addition, the ICO configuration has been reported as the lowest-energy structure for Cu_{13} and Ag_{13},[71,92] which is not supported by our calculations.

Previous first-principles DFT calculations have reported an ideal or slightly distorted ICO configuration for Ni_{13}. In contrast with those studies,[57,67,69] we found a less compact structure that is 0.27 eV lower in energy than the ideal ICO structure. This result indicates that Ni_{13} has a structure much closer to the Co_{13} HBL structure. However, its relative energy difference with respect to the ideal ICO cluster is only a fraction of the obtained for Co_{13} (−1.14 eV). Thus, it shows that our approach is able to identify new lower energy structures for the M_{13} clusters.

A DSC-like structure yields the lowest-energy configuration for four systems, namely, Ru_{13}, Rh_{13}, Os_{13}, and Ir_{13}, which are neighbors in the periodic table. DSC is composed by three planes stacked as in the simple-cubic structure (12 atoms), and the 13th atom is add to the 12 atoms structure,

and hence, DSC has an open structure due to the simple-cubic stacking. We observed that although the top cube in Os_{13} and Ru_{13} are tilted, it maintains the mirror symmetry. The DSC structure was first proposed for Ir, Ru, Rh, and Pt clusters,[95] which is consistent with our results for Ir_{13}, Ru_{13}, and Rh_{13}, however, our lowest-energy structure for Pt_{13} is about 1.3 eV lower than DSC. We would like to point out that the ideal DSC cluster yields the highest energy for most of the systems that have ICO-like structures, which can be explained by the large preference of those systems to maintain a compact structure.

The Zn_{13} and Cd_{13} systems have very similar structures, which are different from all other systems, i.e., they show signs of disordering that resemble an amorphous system. Similar disordered structures were also reported by previous DFT studies for Zn_{13} and Cd_{13}.[76–78] The ICO structure has also been reported as the lowest-energy structure for Cd_{13},[93] which is clearly not supported by our calculations. The Zn_{13}, Cd_{13}, and Hg_{13} systems have a closed-shell electronic structure ($3d^{10}4s^2$, $4d^{10}4s^2$, and $5d^{10}6s^2$), however, Zn_{13} and Cd_{13} have disordered structures while Hg_{13} has an ordered, high-symmetry ICO structure. Thus, it indicates remarkable differences between those systems due to the degree of localization of the d states.

The structures for Mo_{13}, W_{13}, Pt_{13}, and Au_{13} cannot fit easily in the structure groups mentioned above. It is important to mention that the 3D Au_{13} structure is only stabilized by taken SOC effects into account for the valence electrons, i.e., there is a clear competition between 2D and 3D structures for Au_{13}. In contrast with previous studies,[72] we found an ordered structure for Au_{13}. We identified also local minimum structures with disordered features for Au_{13}, however, are higher in energy. Thus, it can explain the discrepancies with previous results.

E. Effective coordination number and averaged bond lengths

In this section, we will employ the concepts of ECN and average bond lengths, d_{av},[121,122] to analyze the lowest-energy atomic structures. The ECN takes into account that a particular atom i is surrounded by atoms at different distances while the standard coordination number (CN) attributes an unique weight for all bonds independently of their bond lengths. For example, the CN of a particular atom i can be obtained by using a cutoff bond length and counting the number of atoms surrounding atom i with bond lengths smaller than the cutoff value, i.e., all atoms with bond lengths smaller than the cutoff value contribute with the same weight (unit) for CN. Thus, the results obtained for the CN depend on the cutoff bond length. In contrast, a different weight is attributed for each bond length by using a weight function in the ECN concept. For example, bond lengths smaller (larger) than d_{av} contribute with a weight larger (smaller) than the unit. Thus, a cutoff bond length is not required in the ECN concept. For particular cases, the ECN has the same value as the CN, e.g., the average ECN and CN is 6.46 for the ideal ICO cluster. For low-symmetry structures in which a particular atom is surrounded by atoms at different distances, the ECN and CN can assume different values, and its difference (Δ=ECN−CN) depends on the selected cutoff bond length to obtain the CN. Therefore, the ECN concept provides a more accurate approach to identify possible structural trends in clusters.

In this work, we will use an exponential averaging function to obtain ECN_i and d_{av}^i for all atoms in the cluster.[122] The ECN_i is obtained by the following set of equations:

$$\mathrm{ECN}_i = \sum_j \exp\left[1 - \left(\frac{d_{ij}}{d_{av}^i}\right)^6\right], \tag{3}$$

where d_{ij} is the distance between atom i and j, while d_{av}^i is defined as

$$d_{av}^i = \frac{\sum_j d_{ij} \exp\left[1 - \left(\frac{d_{ij}}{d_{av}^i}\right)^6\right]}{\sum_j \exp\left[1 - \left(\frac{d_{ij}}{d_{av}^i}\right)^6\right]} \tag{4}$$

in which d_{av}^i is obtained self-consistently, i.e., $|d_{av}^i(\mathrm{new}) - d_{av}^i(\mathrm{old}) < 0.00010|$. The smallest bond length between the atom i and all j atoms (d_{min}^i) was used as the initial value for d_{av}^i. The final value of d_{av}^i is obtained within three to four iterations, which is then used to obtain ECN_i. The power 6 and exponential form in d_{av}^i are used in order to obtain ECNs equal to the standard CN for undistorted high-symmetric ICO clusters, as well as for crystalline systems with simple lattices such as cubic and face-centered cubic. The average ECN and d_{av} for a particular configuration are obtained by

$$\mathrm{ECN} = \frac{1}{N}\sum_{i=1}^{N} \mathrm{ECN}_i \tag{5}$$

and

$$d_{av} = \frac{1}{N}\sum_{i=1}^{N} d_{av}^i, \tag{6}$$

where N is the total number of atoms in the cluster. All results obtained for ECN and d_{av} are shown in Fig. 5.

It can be seen from Fig. 5 that the ECN depends critically on the cluster configuration. For example, we found a constant value for ECN using ideal ICO clusters for all systems (ECN=6.46), which should be expected, as the geometry of the ideal ICO cluster is constrained by symmetry. Similar trend is observed for the BBP cluster but in this case the ECNs have smaller values due to the arrangement of the atoms in the cluster, which is expected. Most of the values obtained for BBP are about 5.50. However, small oscillations are observed due to the strong preference of few systems (V_{13}, Cr_{13}, Zn_{13}, and Cd_{13}) to have a different configuration.

Using the lowest-energy structures shown in Fig. 4, we concluded that three systems have ideal ICO configuration (Sc_{13}, Y_{13}, and Hg_{13}) and eight systems have distorted ICO-like configurations (Ti_{13}, V_{13}, Cr_{13}, Mn_{13}, Fe_{13}, Zr_{13}, Lu_{13}, and Fe_{13}). For example, we found that nine systems, namely, Sc_{13}, Ti_{13}, Mn_{13}, Fe_{13}, Y_{13}, Zr_{13}, Lu_{13}, Hf_{13}, and Hg_{13} have ECN values close to the ideal ICO clusters (ECN=6.46), which is should be expected, however, two ICO-like systems

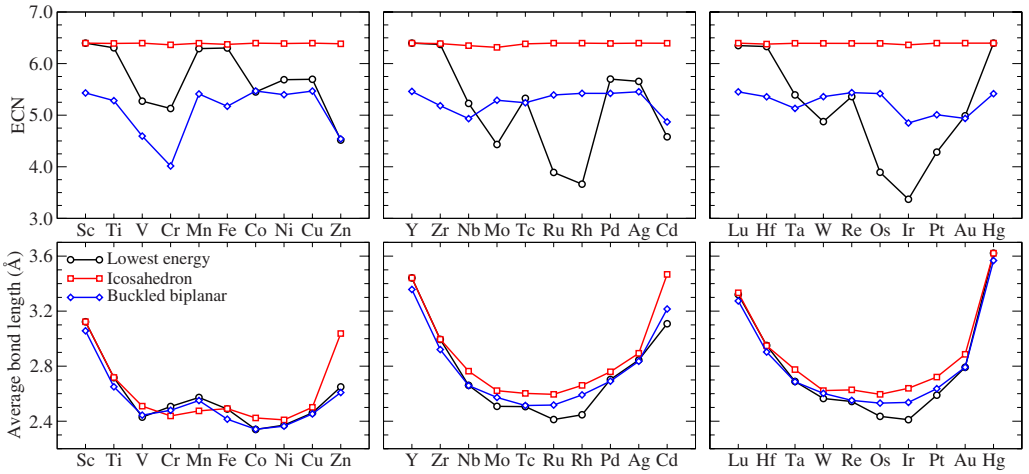

FIG. 5. (Color online) Average bond lengths, d_{av}, and averaged ECN for the lowest-energy clusters, M_{13}, shown in Fig. 4 (black lines, circle), ICO cluster (red lines, square), and BBP (blue lines, diamond).

(V_{13} and Cr_{13}) have ECN values substantially smaller than 6.46. For example, ECN=5.27 and 5.13 for V_{13} and Cr_{13}, respectively.

We found one $3d$ (Zn_{13}), four $4d$ (Mo_{13}, Ru_{13}, Rh_{13}, and Cd_{13}), and five $5d$ (W_{13}, Os_{13}, Ir_{13}, Pt_{13}, and Au_{13}) systems with ECN smaller than five. Thus, it shows clearly that the $3d$ systems have a strong tendency to form compact structures while the $5d$ systems have a large number of open structures. Thus, these results provide a clear indication of the type of structures that should be searched to identify possible lower energy structures.

The averaged bond lengths calculated for the ICO, BBP, and the lowest-energy configurations are shown in Fig. 5. We found that the average bond length for each element is about the same for the three different structure configurations, i.e., atomic structures with different ECN yield similar average bond lengths for M_{13}. In first approximation, the average bond length versus the atomic number shows a similar parabolic shape for the $3d$, $4d$, and $5d$ systems. We found that the largest bond lengths occurs for systems with small or maximum occupation of the d states while the smallest bond lengths occur about half occupied d states.

For $3d$ systems, we observe a small deviation from a parabolic shape, which is characterized by the presence of two minima separated by a maximum located at Mn_{13}. It is relate to the role played by the magnetic interactions in Cr_{13}, Mn_{13}, and Fe_{13}. For example, for the lowest-energy configurations, the total magnetic moment (m_T) of Cr_{13} and Mn_{13} are 0 and $3\mu_B$ per cluster, i.e., AFM and FIM states, respectively, with bond lengths of 2.51 and 2.57 Å. However, those bond lengths decrease to 2.44 and 2.48 Å for the ideal ICO clusters with m_T of 20 and $33\mu_B$, respectively. Thus, the change from FM to FIM and AFM states contribute to increase the average bond lengths by about 0.1 Å and hence, it explains the maximum at Mn_{13}. Similar maximum exists for the cohesive energy of the $3d$ systems.[120] For the $4d$ and $5d$ systems, the deviations from a parabolic profile occur close to the minimum of the average bond-length curves, at the Ru_{13} and Rh_{13} for $4d$ and Os_{13} and Ir_{13} for $5d$.

The approximate parabolic shape of the average bond-length curves can be explained by the chemistry bonding and antibonding model, in which the occupation of the bonding and antibonding states (d states) in $3d$, $4d$, and $5d$ systems determines the magnitude of the binding energy in the system, hence the magnitude of the bond length.[120] For example, the occupation of the bonding states increases up to the half occupation of the d states, i.e., the bond length tends to decrease while the occupation of the antibonding states leads to an increase in the bond length. However, this picture alone cannot explain the deviations observed in the curves from a complete parabolic shape.

F. Magnetic moments

The total magnetic moments, m_T, of M_{13} are shown in Fig. 6 for all calculated configurations while m_T for the ICO, CUBO, BBP, HBL, DSC, and lowest-energy configurations are also summarized in Table I. Figure 6 shows that the range of values obtained for m_T are wider for $3d$, followed by the $4d$ and $5d$ series, which can be related to the large number of magnetic $3d$ bulk systems, e.g., bulk Fe, which is not the case of the $4d$ and $5d$ systems.

Except few differences, we found that m_T versus the atomic number shows similar shape for both $3d$, $4d$, and $5d$ systems. From low to high atomic numbers (left to right in Fig. 6), we observe initially a decreasing in m_T for the first four elements in the three series, i.e., it decreases from $m_T=19(Sc_{13})$, $19(Y_{13})$, and $13\mu_B$ (Lu_{13}) to $m_T=0$ (Cr_{13}), $0(Mo_{13})$, and $0\mu_B$ (W_{13}). Thus, the magnetic interactions change from FM to AFM by increasing the atomic number from left to right for the first four elements. Once m_T reaches its minimum, m_T increases again and reaches its maximum at Fe_{13} ($m_T=44\mu_B$, FM), Rh_{13} ($m_T=9\mu_B$, FIM), and Re_{13} ($m_T=5\mu_B$, FIM). Then, m_T decreases almost linearly with the occupation of the d states and reaches $m_T=0\mu_B$ for Zn_{13}, Cd_{13}, and Hg_{13}.

For the $5d$ systems, m_T decreases exactly by one unit from Re_{13} to Hg_{13}, which does not occur for the $3d$ and $4d$ systems. In particular, the shape of the $3d$ curve from V_{13} to Cu_{13} resembles the Pauling-Slater curve.[120] Hence, these curves are mainly determined by the occupation of the d states while the larger localization of the $3d$ states contrib-

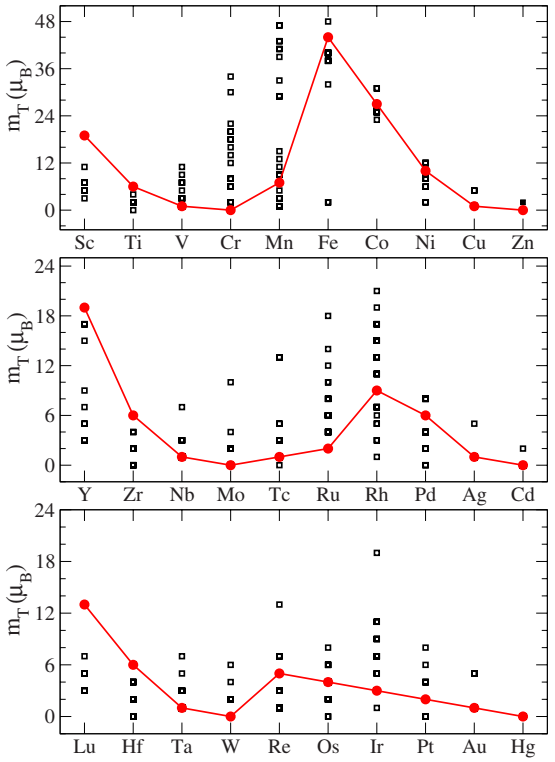

FIG. 6. (Color online) Total magnetic moments, m_T, of the M_{13} clusters given for all calculated structures (open square). m_T for the lowest-energy configurations are indicated in red (full circles).

utes to enhance the magnetic interactions and explains the high magnetic moments obtained for the FM 3*d* configurations. It is important to notice that several systems have nonzero magnetic moments, even when their bulk phases do not show magnetism, e.g., Cu_{13}, Pd_{13}, Pt_{13}, and Au_{13}. These findings can be attributed to the low dimension and lower coordination of those clusters, which have been known to enhance the magnetic properties of surfaces.

For particular systems, a large number of discrepancies between DFT calculations and experimental results have been reported. For Rh_{13}, first-principles calculations have reported m_T=21.0,[83] 17.0,[62,86] 9.0,[46] and 13.0μ_B (Ref. 87) while we found m_T=9.0μ_B. The reported experimental values are 11.44 ± 1.69 (Ref. 31) and 6.24 ± 1.69,[33] i.e., only the most recent DFT studies have obtained m_T in the range of the experimental values. A simple analysis of Table I shows that compact structures for Rh_{13} have higher magnetic moments, e.g., m_T=19μ_B for ICO, which explains those discrepancies between experimental and theory for Rh_{13} as most of the first calculations were initially done for compact model structures for Rh_{13}.[83] We want to point out that different problems contribute to those discrepancies. For example, small energy difference between configurations with very different magnetic moments can play a role. Furthermore, the well-known limitations in the local and semilocal exchange-correlation functionals might play an important role as well.

G. Vibrational frequencies

It is known that vibrational frequencies (ν_{freq}) can be used to verify that a particular atomic configuration is a local minimum, i.e., all local minimum structures must have only positive ν_{freq} values. Thus, a basic requirement to support our results is to verify whether all M_{13} structures shown in Fig. 4 are true local minimums. We determined ν_{freq} by employing the approach in which the Hessian matrix is calculated using finite differences, as implemented in VASP.[112,113] We use two atomic displacements, i.e., each atom is displaced in each direction by ±0.010 Å. All the $3N-6(N=13)$ vibrational frequencies are shown in Fig. 7. We found that all ν_{freq} are positive for the lowest-energy structures shown in Fig. 4 and hence, all configurations are true local minimum.

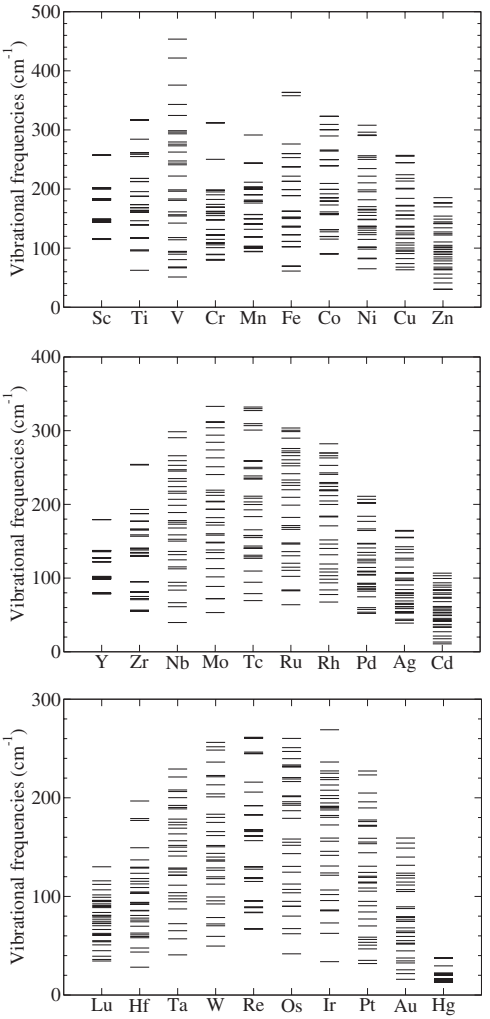

FIG. 7. Vibrational frequencies ($3N-6$) of the lowest-energy structures shown in Fig. 4 for the TM_{13} clusters.

It can be seen that the vibrational frequencies range, i.e., from ν_{freq}^{min} to ν_{freq}^{max}, depends on the series and column in the periodic table. For almost all systems, we found that ν_{freq}^{max} in the same column follows the relationship below

$$\nu_{freq}^{3d\text{-}max} > \nu_{freq}^{4d\text{-}max} > \nu_{freq}^{5d\text{-}max}. \quad (7)$$

Furthermore, in particular, for the 4*d* and 5*d* systems, it can be seen that ν_{freq}^{max} has a parabolic shape as a function of the atomic number, which can be correlated with the binding-energy magnitude.

TABLE III. Comparison of our results (ΔE_{tot}, ECN, and d_{av}) with the results obtained from the atomic structures reported by Sun *et al.* (Ref. 78). The numbers in parentheses indicate the results obtained from Sun *et al.* structures as provided while the results on the right were obtained by performing a geometric relaxation of those structures within the same computational parameters as those used in this work.

	This work			Reference 78		
M_{13}	ΔE_{tot} (eV)	ECN	d_{av} (Å)	ΔE_{tot} (eV)	ECN	d_{av} (Å)
Zn	−1.90	4.52	2.65	(−1.59) −1.90	(4.76) 4.51	(2.57) 2.65
Y	0.00	6.40	3.44	(+0.03) 0.00	(6.40) 6.40	(3.47) 3.44
Zr	−0.08	6.37	2.99	(+0.32) +0.03	(6.24) 6.32	(2.95) 2.99
Nb	−1.48	5.23	2.66	(−1.45) −1.48	(5.26) 5.23	(2.68) 2.66
Mo	−2.57	4.43	2.51	(−2.57) −2.57	(4.43) 4.43	(2.51) 2.51
Tc	−3.46	5.33	2.51	(−2.73) −3.46	(5.24) 5.32	(2.56) 2.51
Ru	−3.20	3.89	2.41	(−2.34) −3.19	(3.64) 3.89	(2.45) 2.41
Rh	−1.31	3.66	2.45	(−1.30) −1.31	(3.66) 3.66	(2.44) 2.45
Pd	−0.32	5.70	2.70	(−0.05) −0.09	(6.36) 6.36	(2.78) 2.76
Ag	−1.25	5.65	2.84	(−0.96) −1.25	(5.71) 5.66	(2.77) 2.85
Cd	−0.69	4.58	3.11	(−0.60) −0.69	(4.78) 4.63	(3.21) 3.12
Ta	−0.85	5.39	2.69	(−0.85) −0.85	(5.39) 5.39	(2.69) 2.69
W	−4.32	4.88	2.57	(−4.05) −4.05	(4.52) 4.52	(2.54) 2.54
Re	−5.76	5.36	2.54	(−5.62) −5.75	(5.32) 5.41	(2.52) 2.54
Os	−6.26	3.89	2.44	(−6.26) −6.26	(3.89) 3.89	(2.43) 2.43
Ir	−6.68	3.37	2.41	(−6.68) −6.68	(3.37) 3.37	(2.41) 2.41
Pt	−3.53	4.28	2.59	(−3.44) −3.44	(4.82) 4.82	(2.61) 2.61

The calculated ν_{freq} are in qualitative agreement with available experimental results for clusters with similar size. For example, experimental results for the vibrational spectrum of neutral Au_7, Au_{19}, and Au_{20} show frequencies between 47 and 220 cm^{-1} (Ref. 10) while we obtained ν_{freq} between 16 and 160 cm^{-1}.

IV. DISCUSSION AND SUMMARY

In this work, we reported a theoretical study of metal M_{13} clusters along of the 3*d*, 4*d*, and 5*d* series based on first-principles calculations without (DFT-PBE) and with SOC (DFT-PBE+SOC) as implemented in VASP. Using a combination of first-principles high-*T* MD simulations, structure crossover, and a set of five well-known configurations, we calculated about 15–45 configurations for each system. A set of lowest-energy structures were identified and are shown in Fig. 4. Vibrational frequency analysis shows that those lower energy configurations are true local minimum structures. We found that SOC was decisive to change the atomic configuration of Au_{13} from 2D to 3D while for all the remaining systems the results are the same as those obtained with DFT-PBE.

Our results are in quite good agreement with previous theoretical calculations[78] based on the combination of TSDS with DFT calculations employing VASP and GAUSSIAN03 codes. We calculated the ΔE_{tot}, ECN, and d_{av} for all the lowest-energy atomic configurations as provided by Sun *et al.*[78] using the same computational parameters as those used in this work. First, no additional relaxations were performed on the provided structures in order to check possible differences due to the atomic relaxation procedure. Subsequently, we performed a full relaxation of the provided structures as performed in this work. All results are summarized in Table III. Compared with the unrelaxed structures, we found that at least nine of our configurations (Zn_{13}, Zr_{13}, Tc_{13}, Ru_{13}, Pd_{13}, Ag_{13}, W_{13}, Re_{13}, and Pt_{13}) are lower in energy by about 0.10–0.80 eV while the remaining systems (Y_{13}, Nb_{13}, Mo_{13}, Rh_{13}, Cd_{13}, Ta_{13}, Os_{13}, and Ir_{13}) yield almost the same relative energy differences, Table III. For those nine systems, we noticed large deviations in the values of ECN and d_{av} compared with our results, which might explain those differences. A full relaxation of Sun *et al.* structures lowers the total energy and provide a better agreement of the ΔE_{tot}, ECN, and d_{av} with our results, however, the differences in ΔE_{tot} are still present for three systems. Our equilibrium configurations for three systems (Pd_{13}, W_{13}, and Pt_{13}) have lower energies than Sun *et al.* by about 0.3 eV. Sun *et al.* suggested a slightly distorted ICO structure for Pd_{13}(ECN=6.36) while our lower energy Pd_{13} structure has an ECN of 5.70, which indicates a slightly more open structure. Therefore, compared with the most recent and complete study,[78] we found three lower energy configurations among 17 common systems. Thus, this work summarizes the best known structures for the M_{13} clusters.

The lowest-energy structures shown in Fig. 4 indicate clear trends. For example, compact ICO-like structures are obtained at the beginning of each metal series, which gradually assumes more opened structures by increasing atomic

number. For d states with occupation larger than half, the lowest-energy structures tend to increase their ECNs, which results in compact structures for large occupation of the d states. It is important to notice that the 3d systems have more compact structures than the 4d and 5d series, which can leads to the following conclusion. It has been known that 3d systems have a much localized d state than 5d systems and hence, we can conclude that an increase in the localization of the d states favor much more compact structures. Further investigation could be performed using the LDA+U framework with different values of the effective Hubbard U term.[15]

Therefore, the structural pattern of the M_{13} clusters are different from the respective bulk systems. For example, with few exceptions, the 3d, 4d, and 5d elements crystallize in the face-centered-cubic, body-centered-cubic, and hexagonal close-packed structures, which are compact structures with large coordination numbers.[4] However, as mentioned above, the ECN results show a strong dependence with the occupation of the d states, specially for the 4d and 5d systems, Fig. 5. In particular, the lowest ECN occurs for systems with face-centered-cubic structures, e.g., Rh, Pd, Ir, and Pt. Thus, the open structures observed for these systems can be considered as unexpected ones, i.e., there is no simple explanation to support the DSC structures for those systems. It is important to notice that compact Rh_{13} have large magnetic moments, which is not consistent with experimental observations while open structures yield m_T in agreement with experimental results.

We want to point out that the binding energy per atom and average bond lengths follow a parabolic shape, as a function of the occupation of the d states. Thus, the same trends observed for bulk systems are observed for few properties of the M_{13} clusters, which indicate that the same mechanism used to explain similar trends in the bulk phase can be applied to explain these particular trends for the M_{13} clusters. In bulk phase, the paraboliclike shape of physical properties have been explained by the bonding and antibonding chemistry picture in which the occupation of the d states and the s-d hybridization determine the magnitude of the mentioned physical properties.[120] The d states in the 3d, 4d, and 5d series is divided into two regions with different characteristics. The bonding states are located at lower energy while the antibonding states are higher in energy. Thus, by increasing the occupation of the bonding states, we expected a decreasing in the average bond length, which is in fact observed in our calculations. Once the bonding states are fully occupied, the minimum bonding length is obtained. The initial occupation of the antibonding states increases the bonding length once again up to reach its maximum value. The atomic structure of the lowest-energy configurations for all calculated systems can be obtained under request.

ACKNOWLEDGMENTS

First, we would like to thank very much René Fournier for providing us all the lowest-energy structures reported in Ref. 78, otherwise a realistic comparison between our studies would not be possible. Maurício J. Piotrowski and Paulo Piquini are thankful to the Brazilian financial agencies CNPq and CAPES while Juarez L. F. Da Silva thanks the São Paulo Science Foundation (FAPESP) for the financial support. Most of the calculations were performed at the National Center of High Performance Computing in Campinas (CENAPAD), calculations for few systems were performed at the National Renewable Energy Laboratory, and all DFT-PBE+SOC calculations were performed in Institute of Physics of São Carlos using the resources provided by FAPESP.

*Corresponding author; dasilva_juarez@yahoo.com

[1] W. A. de Heer, Rev. Mod. Phys. **65**, 611 (1993).
[2] J. A. Alonso, Chem. Rev. **100**, 637 (2000).
[3] F. Baletto and R. Ferrando, Rev. Mod. Phys. **77**, 371 (2005).
[4] C. Kittel, *Introduction to Solid State Physics*, 7th ed. (Wiley, New York, 1996).
[5] A. W. Castleman, Jr. and P. Jena, Proc. Natl. Acad. Sci. U.S.A. **103**, 10554 (2006).
[6] M. Turner, V. B. Golovko, O. P. H. Vaughan, P. Abdulkin, A. Berenguer-Murcia, M. S. Tikhov, B. F. G. Johnson, and R. M. Lambert, Nature (London) **454**, 981 (2008).
[7] A. Wijaya, S. B. Schaffer, I. G. Pallares, and K. Hamad-Schifferli, ACS Nano **3**, 80 (2009).
[8] B. Hvolbæk, T. V. W. Janssens, B. S. Clausen, H. Falsig, C. H. Christensen, and J. K. Nørskov, Nanotoday **2**, 14 (2007).
[9] H. Falsig, B. Hvolbæk, I. S. Kristensen, T. Jiang, T. Bligaard, C. H. Christensen, and J. K. Nøskov, Angew. Chem., Int. Ed. **47**, 4835 (2008).
[10] P. Gruene, D. M. Rayner, B. Redlich, A. F. G. van der Meer, J. T. Lyon, G. Meijer, and A. Fielicke, Science **321**, 674 (2008).
[11] G. Schmid, Chem. Soc. Rev. **37**, 1909 (2008).
[12] M. Walter, J. Akola, O. Lopez-Acevedo, P. D. Jadzinsky, G. Calero, C. J. Ackerson, R. L. Whetten, H. Grönbeck, and H. Häkkinen, Proc. Natl. Acad. Sci. U.S.A. **105**, 9157 (2008).
[13] A. Trovarelli, *Catalysis by Ceria and Related Materials*, 1st ed. (World Scientific, Singapore, 2002).
[14] J. L. F. Da Silva, M. V. Ganduglia-Pirovano, J. Sauer, V. Bayer, and G. Kresse, Phys. Rev. B **75**, 045121 (2007).
[15] J. L. F. Da Silva, Phys. Rev. B **76**, 193108 (2007).
[16] M. V. Ganduglia-Pirovano, J. L. F. Da Silva, and J. Sauer, Phys. Rev. Lett. **102**, 026101 (2009).
[17] J. Kašpar, P. Fornasiero, and N. Hickey, Catal. Today **77**, 419 (2003).
[18] V. Del Colle, A. Berná, G. Tremiliosi-Filho, E. Herrero, and J. M. Feliu, Phys. Chem. Chem. Phys. **10**, 3766 (2008).
[19] J. F. Gomes, B. Busson, A. Tadjeddine, and G. Tremiliosi-Filho, Electrochim. Acta **53**, 6899 (2008).
[20] S. C. Tsang, N. Cailuo, W. Oduro, A. T. S. Kong, L. Clifton, K. M. K. Yu, B. Thiebaut, J. Cookson, and P. Bishop, ACS Nano **2**, 2547 (2008).
[21] X. Pan, Z. Fan, W. Chen, Y. Ding, H. Luo, and X. Bao, Nature Mater. **6**, 507 (2007).

[22] S. Vajda *et al.*, Nature Mater. **8**, 213 (2009).
[23] N. Toshima, Pure Appl. Chem. **72**, 317 (2000).
[24] H. M. Lee, M. Ge, B. R. Sahu, P. Tarakeshwar, and K. S. Kim, J. Phys. Chem. B **107**, 9994 (2003).
[25] G. Wang, M. A. Van Hove, P. N. Ross, and M. I. Baskes, J. Chem. Phys. **121**, 5410 (2004).
[26] H. B. Liu, U. Pal, and J. A. Ascencio, J. Phys. Chem. C **112**, 19173 (2008).
[27] S. Alayoglu, A. U. Nilekar, M. Mavrikakis, and B. Eichhorn, Nature Mater. **7**, 333 (2008).
[28] F. C. Meunier, ACS Nano **2**, 2441 (2008).
[29] D. E. Bergeron, A. W. Castleman, Jr., T. Morisato, and S. N. Khanna, Science **304**, 84 (2004).
[30] P. J. Roach, W. H. Woodward, A. W. Castlman, Jr., A. C. Reber, and S. N. Khanna, Science **323**, 492 (2009).
[31] A. J. Cox, J. G. Louderback, and L. A. Bloomfield, Phys. Rev. Lett. **71**, 923 (1993).
[32] B. V. Reddy, S. N. Khanna, and B. I. Dunlap, Phys. Rev. Lett. **70**, 3323 (1993).
[33] A. J. Cox, J. G. Louderback, S. E. Apsel, and L. A. Bloomfield, Phys. Rev. B **49**, 12295 (1994).
[34] M. B. Knickelbein, Phys. Rev. B **71**, 184442 (2005).
[35] Y. T. Jeon and G. H. Lee, J. Appl. Phys. **103**, 094313 (2008).
[36] S. E. Apsel, J. W. Emmert, J. Deng, and L. A. Bloomfield, Phys. Rev. Lett. **76**, 1441 (1996).
[37] J. Guevara, A. M. Llois, and M. Weissmann, Phys. Rev. Lett. **81**, 5306 (1998).
[38] M. Sakurai, K. Watanabe, K. Sumiyama, and K. Suzuki, J. Chem. Phys. **111**, 235 (1999).
[39] H. K. Yuan, H. Chen, A. S. Ahmed, and J. F. Zhang, Phys. Rev. B **74**, 144434 (2006).
[40] C. D. Dong and X. G. Gong, Phys. Rev. B **78**, 020409(R) (2008).
[41] A. L. Mackay, Acta Crystallogr. **15**, 916 (1962).
[42] D. C. Douglass, J. P. Bucher, and L. A. Bloomfield, Phys. Rev. B **45**, 6341 (1992).
[43] M. B. Knickelbein, Phys. Rev. Lett. **86**, 5255 (2001).
[44] M. B. Knickelbein, Phys. Rev. B **70**, 014424 (2004).
[45] X. Xu, S. Yin, R. Moro, and W. A. de Heer, Phys. Rev. Lett. **95**, 237209 (2005).
[46] Y.-C. Bae, V. Kumar, H. Osanai, and Y. Kawazoe, Phys. Rev. B **72**, 125427 (2005).
[47] J. Wang, Phys. Rev. B **75**, 155422 (2007).
[48] S.-Y. Wang, J.-Z. Yu, H. Mizuseki, J.-A. Yan, Y. Kawazoe, and C.-Y. Wang, J. Chem. Phys. **120**, 8463 (2004).
[49] P. Alvarado, J. Dorantes-Dávila, and H. Dreyssé, Phys. Rev. B **50**, 1039 (1994).
[50] A. Taneda, T. Shimizu, and Y. Kawazoe, J. Phys.: Condens. Matter **13**, L305 (2001).
[51] H. Cheng and L.-S. Wang, Phys. Rev. Lett. **77**, 51 (1996).
[52] P. Bobadova-Parvanova, K. A. Jackson, S. Srinivas, and M. Horoi, Phys. Rev. A **67**, 061202(R) (2003).
[53] P. Bobadova-Parvanova, K. A. Jackson, S. Srinivas, and M. Horoi, J. Chem. Phys. **122**, 014310 (2005).
[54] B. I. Dunlap, Phys. Rev. A **41**, 5691 (1990).
[55] P. Bobadova-Parvanova, K. A. Jackson, S. Srinivas, and M. Horoi, Phys. Rev. B **66**, 195402 (2002).
[56] O. Šipr, M. Košuth, and H. Ebert, Phys. Rev. B **70**, 174423 (2004).
[57] R. Singh and P. Kroll, Phys. Rev. B **78**, 245404 (2008).
[58] Z.-Q. Li and B.-L. Gu, Phys. Rev. B **47**, 13611 (1993).
[59] K. Miura, H. Kimura, and S. Imanaga, Phys. Rev. B **50**, 10335 (1994).
[60] S.-R. Liu, H.-J. Zhai, and L.-S. Wang, Phys. Rev. B **64**, 153402 (2001).
[61] J. L. Rodríguez-López, F. Aguilera-Granja, K. Michaelian, and A. Vega, Phys. Rev. B **67**, 174413 (2003).
[62] C. M. Chang and M. Y. Chou, Phys. Rev. Lett. **93**, 133401 (2004).
[63] L. Zhan, J. Z. Y. Chen, W.-K. Liu, and S. K. Lai, J. Chem. Phys. **122**, 244707 (2005).
[64] F. Aguilera-Granja, J. M. Montejano-Carrizalez, and R. A. Guirado-López, Phys. Rev. B **73**, 115422 (2006).
[65] L.-L. Wang and D. D. Johnson, Phys. Rev. B **75**, 235405 (2007).
[66] E. K. Parks, L. Zhu, J. Ho, and S. J. Riley, J. Chem. Phys. **100**, 7206 (1994).
[67] F. A. Reuse and S. N. Khanna, Chem. Phys. Lett. **234**, 77 (1995).
[68] F. Aguilera-Granja, S. Bouarab, M. J. López, A. Vega, J. M. Montejano-Carrizales, M. P. Iñiguez, and J. A. Alonso, Phys. Rev. B **57**, 12469 (1998).
[69] T. Futschek, J. Hafner, and M. Marsman, J. Phys.: Condens. Matter **18**, 9703 (2006).
[70] R. C. Longo and L. J. Gallego, Phys. Rev. B **74**, 193409 (2006).
[71] Ş. Erkoç and R. Shaltaf, Phys. Rev. A **60**, 3053 (1999).
[72] J. Oviedo and R. E. Palmer, J. Chem. Phys. **117**, 9548 (2002).
[73] E. M. Fernández, J. M. Soler, I. L. Garzón, and L. C. Balbás, Phys. Rev. B **70**, 165403 (2004).
[74] C. R. Hsing, C. M. Wei, N. D. Drummond, and R. J. Needs, Phys. Rev. B **79**, 245401 (2009).
[75] V. L. Mazalova, A. V. Soldatov, S. Adam, A. Yakovlev, T. Möller, and R. L. Johnston, J. Phys. Chem. C **113**, 9086 (2009).
[76] K. Michaelian, M. R. Beltrán, and I. L. Garzón, Phys. Rev. B **65**, 041403(R) (2002).
[77] J. Wang, G. Wang, and J. Zhao, Phys. Rev. A **68**, 013201 (2003).
[78] Y. Sun, M. Zhang, and R. Fournier, Phys. Rev. B **77**, 075435 (2008).
[79] D. Kaiming, Y. Jinlong, X. Chuanyun, and W. Kelin, Phys. Rev. B **54**, 11907 (1996).
[80] V. Kumar and Y. Kawazoe, Phys. Rev. B **65**, 125403 (2002).
[81] S. Li, H. Li, J. Liu, X. Xue, Y. Tian, H. He, and Y. Jia, Phys. Rev. B **76**, 045410 (2007).
[82] Y. Jinlong, F. Toigo, W. Kelin, and Z. Manhong, Phys. Rev. B **50**, 7173 (1994).
[83] B. V. Reddy, S. K. Nayak, S. N. Khanna, B. K. Rao, and P. Jena, Phys. Rev. B **59**, 5214 (1999).
[84] R. Guirado-López, P. Villaseñor-González, J. Dorantes-Dávila, and G. M. Pastor, J. Appl. Phys. **87**, 4906 (2000).
[85] F. Aguilera-Granja, J. L. Rodríguez-López, K. Michaelian, E. O. Berlanga-Ramírez, and A. Vega, Phys. Rev. B **66**, 224410 (2002).
[86] Y.-C. Bae, H. Osanai, V. Kumar, and Y. Kawazoe, Phys. Rev. B **70**, 195413 (2004).
[87] J. Rogan, G. García, C. Loyola, W. Orellana, R. Ramírez, and M. Kiwi, J. Chem. Phys. **125**, 214708 (2006).
[88] N. Watari and S. Ohnishi, Phys. Rev. B **58**, 1665 (1998).
[89] M. Moseler, H. Häkkinen, R. N. Barnett, and U. Landman, Phys. Rev. Lett. **86**, 2545 (2001).
[90] V. Kumar and Y. Kawazoe, Phys. Rev. B **66**, 144413 (2002).
[91] F. Aguilera-Granja, A. Vega, J. Rogan, W. Orellana, and G.

García, Eur. Phys. J. D **44**, 125 (2007).
[92] J. Zhao, Y. Luo, and G. Wang, Eur. Phys. J. D **14**, 309 (2001).
[93] J. Zhao, Phys. Rev. A **64**, 043204 (2001).
[94] T. Başţuğ, Ş. Erkoç, M. Hirata, and S. Tachimori, Phys. Rev. A **59**, 3690 (1999).
[95] W. Zhang, L. Xiao, Y. Hirata, T. Pawluk, and L. Wang, Chem. Phys. Lett. **383**, 67 (2004).
[96] E. Aprà and A. Fortunelli, J. Phys. Chem. A **107**, 2934 (2003).
[97] L. Xiao and L. Wang, J. Phys. Chem. A **108**, 8605 (2004).
[98] V. Kumar and Y. Kawazoe, Phys. Rev. B **77**, 205418 (2008).
[99] R. Arratia-Perez, A. F. Ramos, and G. L. Malli, Phys. Rev. B **39**, 3005 (1989).
[100] O. D. Häberlen, S.-C. Chung, M. Stener, and N. Rösch, J. Chem. Phys. **106**, 5189 (1997).
[101] F. Furche, R. Ahlrichs, P. Weis, C. Jacob, and S. Gilb, J. Chem. Phys. **117**, 6982 (2002).
[102] H. Häkkinen, B. Yoon, U. Landman, X. Li, H.-J. Zhai, and L.-S. Wang, J. Phys. Chem. A **107**, 6168 (2003).
[103] E. Aprà, R. Ferrando, and A. Fortunelli, Phys. Rev. B **73**, 205414 (2006).
[104] Y. Wang, H.-J. Flad, and M. Dolg, Phys. Rev. B **61**, 2362 (2000).
[105] B. Hartke, H.-J. Flad, and M. Dolg, Phys. Chem. Chem. Phys. **3**, 5121 (2001).
[106] P. Hohenberg and W. Kohn, Phys. Rev. **136**, B864 (1964).
[107] W. Kohn and L. J. Sham, Phys. Rev. **140**, A1133 (1965).
[108] J. P. Perdew, J. A. Chevary, S. H. Vosko, K. A. Jackson, M. R. Pederson, D. J. Singh, and C. Fiolhais, Phys. Rev. B **46**, 6671 (1992).
[109] J. P. Perdew, K. Burke, and M. Ernzerhof, Phys. Rev. Lett. **77**, 3865 (1996).
[110] P. E. Blöchl, Phys. Rev. B **50**, 17953 (1994).
[111] G. Kresse and D. Joubert, Phys. Rev. B **59**, 1758 (1999).
[112] G. Kresse and J. Hafner, Phys. Rev. B **48**, 13115 (1993).
[113] G. Kresse and J. Furthmüller, Phys. Rev. B **54**, 11169 (1996).
[114] M. N. Huda, M. K. Niranjan, B. R. Sahu, and L. Kleinman, Phys. Rev. A **73**, 053201 (2006).
[115] J.-O. Joswig and M. Springborg, Phys. Rev. B **68**, 085408 (2003).
[116] D. J. Wales and J. P. K. Doye, J. Phys. Chem. A **101**, 5111 (1997).
[117] H. G. Kim, S. K. Choi, and H. M. Lee, J. Chem. Phys. **128**, 144702 (2008).
[118] J. Cheng and R. Fournier, Theor. Chem. Acc. **112**, 7 (2004).
[119] T. Futschek, M. Marsman, and J. Hafner, J. Phys.: Condens. Matter **17**, 5927 (2005).
[120] W. A. Harrison, *Electronic Structure and the Properties of Solids: The Physics of the Chemical Bond* (Dover, New York, 1980).
[121] R. Hoppe, Angew. Chem., Int. Ed. Engl. **9**, 25 (1970).
[122] R. Hoppe, Z. Kristallogr. **150**, 23 (1979).